Letter

Melting phase diagram of bubble phases in high Landau levels

K. A. Villegas Rosales, S. K. Singh, H. Deng, Y. J. Chung, L. N. Pfeiffer, K. W. West, K. W. Baldwin, and M. Shayegan
Department of Electrical Engineering, Princeton University, Princeton, New Jersey 08544, USA

(Received 4 July 2021; accepted 31 August 2021; published 20 September 2021)

A low-disorder, two-dimensional electron system (2DES) subjected to a large perpendicular magnetic field and cooled to very low temperatures provides a rich platform for studies of many-body quantum phases. The magnetic field quenches the electrons' kinetic energy and quantizes the energy into a set of Landau levels, allowing the Coulomb interaction to dominate. In excited Landau levels, the fine interplay between short- and long-range interactions stabilizes bubble phases, Wigner crystals with more than one electron per unit cell. Here, we present the screening properties of bubble phases, probed via a simple capacitance technique where the 2DES is placed between a top and a bottom gate and the electric field penetrating through the 2DES is measured. The bubbles formed at very low temperatures screen the electric field poorly as they are pinned by the residual disorder potential, allowing a large electric field to reach the top gate. As the temperature is increased, the penetrating electric field decreases and, surprisingly, exhibits a pronounced minimum at a temperature that appears to coincide with the melting temperature of the bubble phase. We deduce a quantitative phase diagram, as a function of Landau level filling factor (ν) and temperature, for the transition from the bubble to liquid phases for $4 \leqslant \nu \leqslant 5$.

DOI: 10.1103/PhysRevB.104.L121110

Two-dimensional electron systems (2DESs) in a perpendicular magnetic field reveal a fascinating set of many-body quantum phases [1–3]. In the lowest orbital Landau level (LL), there is a plethora of fractional quantum Hall states. In excited LLs, however, the nodes in the wave function lead to a weakened short-range interaction and a preferred long-range order, manifested by the formation of charge-density-wave and stripe/nematic phases [4–9]. Consistent with this expectation, magnetotransport data for very low-disorder 2DESs at very low temperatures have revealed anisotropic phases at half-filled, high-index LLs [10,11] which are interpreted as stripe (or nematic) phases. Moreover, away from exact half fillings, e.g., at LL filling factors $\nu \simeq i + 1/4$ and $\simeq i + 3/4$, there are unusual phases with a vanishing longitudinal resistance and a Hall resistance that is quantized at a value corresponding to the nearest integer quantum Hall state (IQHS), namely, at ih/e^2 and $(i+1)h/e^2$, respectively (i is an integer $\geqslant 2$) [12–15]. These are believed to be bubble phases, Wigner crystal states with more than one electron per unit cell, as shown in Fig. 1(a)[1]. Because they are pinned by the small but ubiquitous disorder, they are insulating but phenomenologically appear as reentrant IQHSs (RIQHSs). Even though the bulk of the 2DES is insulating, the longitudinal resistance vanishes because of the conducting edge states of the underlying LLs [see Fig. 1(b)]. Besides magnetotransport, numerous other experimental techniques have been employed to study the bubble phases; these include measurements of nonlinear I-V [12,16,17], microwave resonance [18,19], and surface acoustic waves [20,21]. The results of all these measurements are consistent with the presence of bubble phases.

Here, we present experimental data, probing the bubble phases and their melting into a liquid state, using a technique that measures their screening efficiency. As highlighted in Fig. 1(c), this is a simple capacitance technique [22–25] where the application of an AC voltage between the top and back gates induces an electric field E_P that penetrates through the 2DES. The magnitude of E_P depends on the screening efficiency of the 2DES bulk, and the size of the penetrating current I_P is then probed in response to E_P. At the lowest temperatures, we find that the pinned bubble phases screen the electric field between the gates poorly and a large I_P is observed. With increasing temperature, the screening efficiency of the 2DES improves and I_P drops, as expected. However, I_P shows a distinct minimum at a temperature that corresponds to the melting temperature of the bubble phases. This observation suggests that the bubble phases become particularly efficient at screening near their melting. We use the data to construct a bubble-liquid melting phase diagram as a function of filling factor and temperature.

We studied a 2DES confined to a 30-nm-wide modulation-doped GaAs quantum well grown on a GaAs (001) substrate. The Si dopant atoms were placed in doping wells [26], leading to a very high-quality 2DES. The sample has density $n = 2.96 \times 10^{11}$ cm^{-2} and a low-temperature mobility $\mu \simeq 30 \times 10^6$ cm^2/V s. We measured a 4 mm × 4 mm van der Pauw geometry sample with diffused InSn electrical contacts at the corners. The device is mounted on a header using In that serves as a back gate, and on top has a deposited, semitransparent, 15-nm-thick Al film top gate. We illuminated our sample before the measurements [27]. We used lock-in

[1]In Fig. 1(a), and also in Fig. 2(a) inset, for simplicity we show only schematic *electron* bubble phases. We note that at filling factor $\nu = 4.7$ the expected ground state is a *hole* bubble phase.

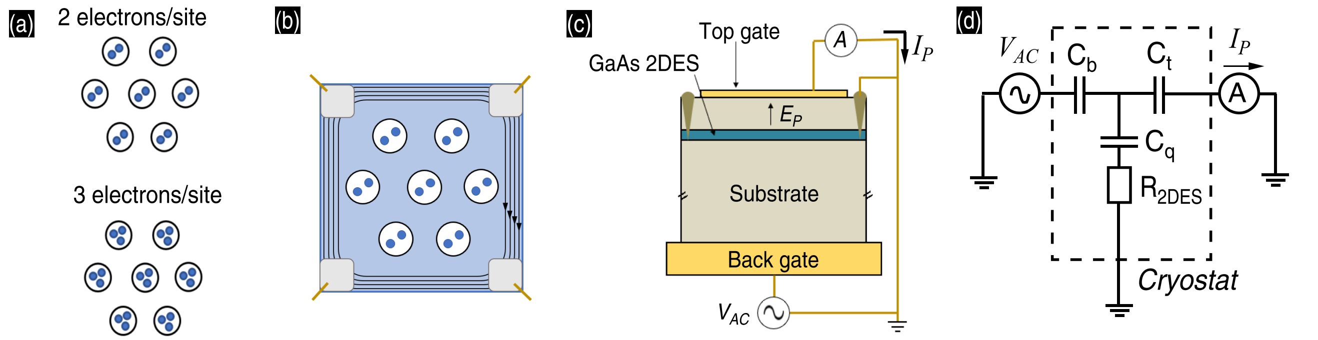

FIG. 1. (a) Schematic representations of bubble phases that have two or three electrons per lattice site. Bubble phases are formed in the excited Landau levels. (b) Measurement geometry (van der Pauw), where the gray squares represent the diffused electrical contacts to the GaAs 2DES. The edge currents flow near the perimeter of the sample, while the bubble phases occupy the bulk of the system. (c) Penetrating electric field measurement setup. An AC excitation voltage ($V_{\rm AC}$) is applied between the top and back gates and the GaAs 2DES screens the established electric field, allowing only a penetrating electric field (E_P) to pass through. From the top gate we collect the penetrating current (I_P) induced by E_P. (d) A lumped-element circuit model of our device. The different components such as back-gate capacitance (C_b), top-gate capacitance (C_t), and the 2DES quantum capacitance (C_q) and resistance ($R_{\rm 2DES}$) are located inside of the cryostat (dashed box).

techniques for magnetoresistance ($\simeq$17 Hz) and capacitance measurements. For the latter, the frequency (f) range was 2 Hz $\lesssim f \lesssim$ 1000 Hz. The sample and a calibrated RuO thermometer next to it were placed on the cold finger of a dry dilution refrigerator.

Figure 2(a) provides magnetoresistance data as a function of ν at the temperature $T \simeq 66$ mK. Near $\nu = 4.3$

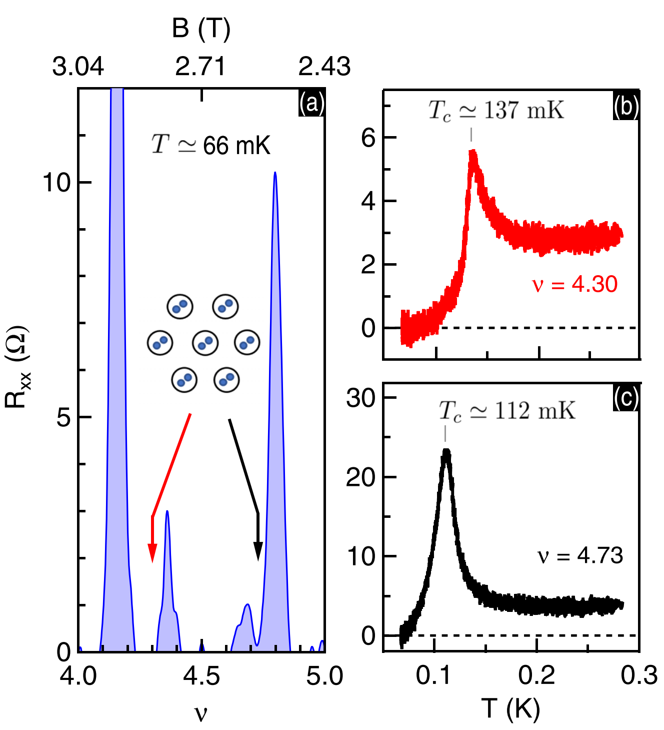

FIG. 2. (a) Longitudinal resistance (R_{xx}) vs Landau level filling factor (ν) for our 2DES with density $n = 2.96 \times 10^{11}$ cm^{-2}, at temperature $T \simeq 66$ mK. The trace represents the resistance along the "easy-axis" direction. The red and black arrows point to the regions where the bubble phases, exhibiting a RIQHS behavior, are observed. The inset shows a bubble phase with 2 electrons/site that forms at the lowest temperatures (see footnote 1). (b) R_{xx} vs T, measured at $\nu = 4.30$ (red) and 4.73 (black). As the temperature is raised, the resistance peaks at T_c.

and 4.7 (marked by arrows), the longitudinal resistance (R_{xx}) has vanishing values and the Hall trace is quantized to the resistance value of the nearest IQHS, signaling a RIQHS behavior [10–14,16,18]. See the Supplemental Material (SM) [28] for R_{yy} and R_{xy} traces. These characteristics have been associated with disorder-pinned bubble phases, which are observed in the highest-quality 2DESs. Pinned bubble phases have vanishingly small conductivity, but in transport measurements, the insulating behavior is shunted by the underlying edge currents of the filled LLs [see, e.g., Fig. 1(b)]. We will return to the temperature dependence of R_{xx} shown in Figs. 2(b) and 2(c) later in this Letter.

By probing the screening efficiency of the 2DES, we derive information regarding its bulk. Figure 3(a) shows the sample's screening efficiency for ν ranging from 4 to 5, at $T \simeq 61$ mK [33]. For the $\nu = 4$ and 5 IQHSs, I_P is a maximum, indicating minimal screening, i.e., an insulating bulk as the quasiparticles are localized by the disorder potential. As ν increases from $\nu = 4$, I_P decreases and reaches a minimum at $\nu \simeq 4.15$, hinting at the presence of delocalized quasiparticles that are able to screen better the penetrating electric field. For larger ν, I_P rises and peaks at $\nu = 4.30$; the local maximum in I_P coincides with the bubble phase region in transport experiments, namely the vanishing of R_{xx} [see Fig. 2(a)]. In pinned electron solids, the electrons are fixed to their positions and are unable to screen effectively the penetrating electric field, thus leading to signatures of minimal screening (maximal I_P) [22,23], as seen in Fig. 3(a) at $\nu \simeq 4.30$. When ν starts at 5 and decreases, I_P follows a similar trend, reaching a local maximum at $\nu \simeq 4.73$.

In between the bubble phases ($4.4 \lesssim \nu \lesssim 4.6$), I_P is minimal. This range of ν coincides with the region where anisotropic stripe/nematic phases are detected in magnetotransport [4–6,9–11] [see Fig. 2(a)]. Stripe/nematic phases are unidirectional charge density waves that are highly conductive along the stripe/nematic direction at finite temperatures, thus an impinging electric field should be screened, in agreement with the local wide I_P minimum seen in Fig. 3(a). Note that we observe the same signatures of pinned bubble

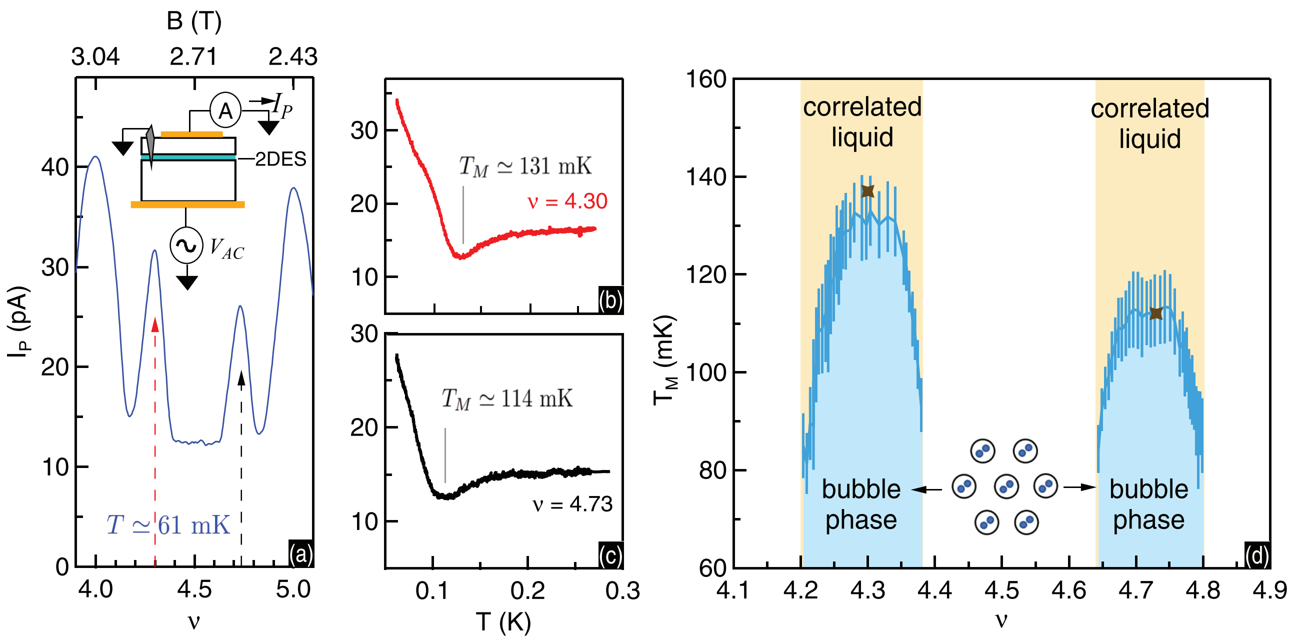

FIG. 3. (a) Penetration current (I_P) vs ν at $T \simeq 61$ mK. The bubble phases are marked by dashed lines. The inset shows the capacitance setup. We apply an AC excitation voltage $V_{\mathrm{AC}} = 10$ mV between the gates at frequency $f = 213$ Hz. (b,c) Temperature dependence of I_P for $\nu = 4.30$ and 4.73. A local minimum in I_P is observed at T_M, which we associate with the melting of the bubble phase. (d) Thermal melting phase diagram for the bubble phases for $4 < \nu < 5$. The blue regions are the bubble phases delimited by T_M. The yellow regions indicate the liquid states at high temperatures. The two brown crosses denote the maxima found in the nonmonotonic temperature dependence of R_{xx} in Figs. 2(b) and 2(c). The cartoon shows a bubble phase with 2 electrons/site.

and stripe/nematic phases in I_P at higher LLs, up to $\nu = 7$ [28].

By measuring I_P at fixed ν as the temperature is raised, we capture the screening behavior of the bubble phases as they melt. Figures 3(b) and 3(c) show I_P vs T for $\nu = 4.30$ and 4.73. At the lowest temperatures, I_P has large values consistent with pinned bubble phases. At high temperatures, I_P saturates at a value that is lower than its maximum low-temperature value, consistent with a melted state, i.e., a liquid phase that has a higher screening efficiency than the pinned bubble phase. One would expect that as the bubbles melt, I_P would change monotonically between these two limits as the electrons become unpinned with increasing temperature. Surprisingly, however, in between these two limits, I_P reaches a local minimum at temperature T_M, implying maximal screening at this temperature [34].

We attempt to understand qualitatively the nonmonotonic I_P response with a lumped-element circuit model as shown in Fig. 1(d) [35]. The 2DES is characterized by its quantum capacitance (C_q) and bulk resistance (R_{2DES}). Since the values of the top and bottom capacitances (C_t and C_b) are fixed, changes in I_P are a direct consequence of variations in the 2DES impedance $Z_{\mathrm{2DES}} = R_{\mathrm{2DES}} + \frac{1}{j\omega C_q}$. The local minimum in I_P, at T_M, implies a dip in Z_{2DES}, which could mean that R_{2DES} decreases, or C_q increases, or both.

We associate T_M with the melting temperature of the bubble phases based on the following considerations. First, a qualitatively similar behavior in I_P vs T traces was recently seen when studying the screening properties of the Wigner crystal at very small ν (*lowest* LL) in low-density GaAs 2D electron and hole systems [22,23]. Associating the temperature for maximum screening with the melting temperature of the Wigner crystal, Ref. [22] found the measured dependence of this temperature on ν to be consistent with the melting phase diagrams reported previously for the Wigner crystal in GaAs 2DESs [36–39]. Second, theories for the melting of a 2D solid [40–43] predict a divergence in the compressibility near the melting temperature. The compressibility is proportional to C_q in Fig. 1(d), and the 2DES screening ability is directly related to Z_{2DES}. A large compressibility would lead to increased screening. We surmise that the maximal screening at our measured T_M might be related to an increase in C_q as the bubble phase melts.

A natural question that arises is whether the nonmonotonic behavior of I_P and the value of T_M are intrinsic to the 2DES and not an artifact of our measurement circuitry. As discussed in the SM [28] we tested this by measuring I_P for frequencies ranging from 21.3 to 1000 Hz. The nonmonotonic I_P behavior and the value of T_M are frequency independent over this range.

Associating T_M with the melting temperature, a plot of our measured T_M vs ν, as shown in Fig. 3(d), provides the bubbles' thermal melting phase diagram. The light-blue and yellow regions represent the bubble phases and correlated liquids, respectively. The error bars give an estimate of the uncertainty in determining the temperature of the local minimum in I_P vs T traces. The left-hand-side bubble-liquid boundary has a relatively broad maximum around $\nu = 4.30$, and on its flanks T_M decreases quickly, reaching values as low as $\simeq$80 mK at $\nu \simeq 4.20$ and $\simeq$4.38. The right-hand-side bubble-liquid boundary also has a broad maximum near $\nu = 4.73$ and, away from this maximum, T_M falls rapidly to $\simeq$80 mK at $\nu \simeq 4.65$ and 4.80. Note that 80 mK is our reliable lower-temperature limit for detecting a minimum in I_P. The ν range of the left-hand-side bubble to the liquid boundary in Fig. 3(d) falls within the available theoretical calculations for the bubble phase stability. Density-matrix renormalization group [8] and Hartree-Fock [44,45] calculations predict $4.23 \leqslant \nu \leqslant 4.39$ and $4.21 \leqslant \nu \leqslant 4.44$, respectively, for the ν window where the bubbles are stable. In the simplest scenario the regions around $\nu = 4.30$ and 4.73 should be particle-hole symmetric (see footnote 1).

The melting of bubble phases has also been studied in transport measurements. Deng *et al.* [14,15] performed resistance measurements in a 2DES of very similar density and mobility to our sample. They showed that in the bubble phases' regime there is a sharp transition in R_{xy} as the temperature decreases. At high temperatures, R_{xy} has the classical Hall resistance value, and as the temperature decreases it quickly transitions to the resistance value of the nearest IQHS. Such a sharp transition was used to define the critical temperature (T_c) for the formation/melting of bubble phases. The longitudinal resistance that accompanies the sharp transition in R_{xy}, has a nonmonotonic behavior and it peaks at the same T_c. The measured T_c in the R_{xx} temperature dependence can therefore be also used to pinpoint the formation/melting of bubble phases. Based on their measured T_c, Deng *et al.* [15] constructed thermal melting phase diagrams for bubble phases between $2 \leqslant \nu \leqslant 4$. Their deduced diagrams also exhibit a dome-shaped boundary, similar to those seen in Fig. 3(d).

It is instructive to compare our results for I_P with the temperature dependence of our R_{xx} data. Figures 2(b) and 2(c) feature R_{xx} vs T for $\nu = 4.30$ and 4.73. At the lowest temperatures R_{xx} is very close to zero, which is a manifestation of pinned bubble phases: The divergent bulk resistance is shunted by the underlying edge currents of the filled LLs. For $T \gtrsim 170$ mK, where the bubble phases have melted and the system is composed of unpinned quasiparticles, R_{xx} reaches a nonzero saturation value. The resistance reaches a maximum at an intermediate temperature T_c similar to what has been reported previously in Refs. [14,15,46,47], as summarized above. In our measurements, we find that T_c is indeed very close to T_M deduced from screening efficiency data [see Figs. 3(b) and 3(c)]. This can be best seen in the phase diagram in Fig. 3(d) where we have added our measured T_c as brown crosses. Note that our measured T_c values coincide (to within 5%) with those reported by Deng *et al.* [14].

Further contrasting of our data can be done with microwave resonance results from a very similar GaAs 2DES, again with comparable density and mobility to ours [18,19]. At $T \simeq 50$ mK, Lewis *et al.* [18] found resonances in the ranges $4.20 \lesssim \nu \lesssim 4.37$ and $4.62 \lesssim \nu \lesssim 4.82$, providing support to the picture of pinned bubble phases. These filling factor ranges overlap with those where we see bubble phases in our experiments [Fig. 3(d)]. Reference [18] also reported that the resonances are strongest at low temperatures and disappear when the temperature exceeds $\simeq$110 mK. This is somewhat smaller than our measured $T_M \simeq 131$ mK. Given our measured T_c and T_M values, it appears that the melting temperatures derived from screening and transport measurements are slightly larger than those from microwave resonances.

In summary, we report screening efficiency measurements of pinned bubble phases in excited LLs. As the bubble phases melt, a minimum in I_P at temperature T_M is found, signaling maximal screening. We associate T_M with the bubble phase melting temperature and construct a melting phase diagram for the bubbles near $\nu = 4.30$ and 4.70. We would like to highlight that the higher screening at an intermediate temperature appears to be a ubiquitous phenomenon for the melting of magnetic-field-induced electron solids formed in 2D systems, be it in the lowest [22,23] or the excited LLs, thus it begs a rigorous theoretical explanation.

Acknowledgments. We acknowledge support by the National Science Foundation (NSF) Grant No. DMR 2104771 for measurements. For sample characterization, we acknowledge support by the U.S. Department of Energy Basic Energy Office of Science, Basic Energy Sciences (Grant No. DEFG02-00-ER45841) and, for sample synthesis, NSF Grants No. ECCS 1906253 and MRSEC No. DMR 1420541, and the Gordon and Betty Moore Foundation's EPiQS Initiative (Grant No. GBMF9615 to L.N.P.). We thank David Huse and Boris Shklovskii for illuminating discussions.

[1] *Perspective in Quantum Hall Effects: Novel Quantum Liquids in Low-Dimensional Semiconductor Structures*, edited by S. Das Sarma and A. Pinczuk (Wiley, New York, 1997).
[2] J. K. Jain, *Composite Fermions* (Cambridge University Press, Cambridge, UK, 2007).
[3] *Fractional Quantum Hall Effects: New Developments*, edited by B. I. Halperin and J. K. Jain (World Scientific, Singapore, 2020).
[4] M. M. Fogler, A. A. Koulakov, and B. I. Shklovskii, Ground state of a two-dimensional electron liquid in a weak magnetic field, Phys. Rev. B **54**, 1853 (1996).
[5] A. A. Koulakov, M. M. Fogler, and B. I. Shklovskii, Charge Density Wave in Two-Dimensional Electron Liquid in Weak Magnetic Field, Phys. Rev. Lett. **76**, 499 (1996).
[6] R. Moessner and J. T. Chalker, Exact results for interacting electrons in high Landau levels, Phys. Rev. B **54**, 5006 (1996).
[7] F. D. M. Haldane, E. H. Rezayi, and K. Yang, Spontaneous Breakdown of Translational Symmetry in Quantum Hall Systems: Crystalline Order in High Landau Levels, Phys. Rev. Lett. **85**, 5396 (2000).
[8] N. Shibata and D. Yoshioka, Ground-State Phase Diagram of 2D Electrons in a High Landau Level: A Density Matrix Renormalization Group Study, Phys. Rev. Lett. **86**, 5755 (2001).
[9] E. Fradkin and S. A. Kivelson, Liquid-crystal phases of quantum Hall systems, Phys. Rev. B **59**, 8065 (1999).
[10] M. P. Lilly, K. B. Cooper, J. P. Eisenstein, L. N. Pfeiffer, and K. W. West, Evidence for an Anisotropic State of Two-Dimensional Electrons in High Landau Levels, Phys. Rev. Lett. **82**, 394 (1999).
[11] R. R. Du, D. C. Tsui, H. L. Stormer, L. N. Pfeiffer, K. W. Baldwin, and K. W. West, Strongly anisotropic transport in higher two-dimensional Landau levels, Solid State Commun. **109**, 389 (1999).
[12] K. B. Cooper, M. P. Lilly, J. P. Eisenstein, L. N. Pfeiffer, and K. W. West, Insulating phases of two-dimensional electrons in high Landau levels: Observation of sharp thresholds to conduction, Phys. Rev. B **60**, R11285 (1999).

[13] J. P. Eisenstein, K. B. Cooper, L. N. Pfeiffer, and K. W. West, Insulating and Fractional Quantum Hall States in the First Excited Landau level, Phys. Rev. Lett. **88**, 076801 (2002).
[14] N. Deng, J. D. Watson, L. P. Rokhinson, M. J. Manfra, and G. A. Csathy, Contrasting energy scales of reentrant integer quantum Hall states, Phys. Rev. B **86**, 201301(R) (2012).
[15] N. Deng, A. Kumar, M. J. Manfra, L. N. Pfeiffer, K. W. West, and G. A. Csathy, Collective Nature of the REentrant Integer Quantum Hall States in the Second Landau Level, Phys. Rev. Lett. **108**, 086803 (2012).
[16] X. Wang, H. Fu, L. Du, X. Liu, P. Wang, L. N. Pfeiffer, K. W. West, R.-R. Du, and X. Lin, Depinning transition of bubble phases in a high Landau level, Phys. Rev. B **91**, 115301 (2015).
[17] K. Bennaceur, C. Lupien, B. Reulet, G. Gervais, L. Pfeiffer, and K. West, Competing Charge Density Waves Probed by Nonlinear Transport and Noise in the Second and Third Landau Levels, Phys. Rev. Lett. **120**, 136801 (2018).
[18] R. M. Lewis, P. D. Ye, L. W. Engel, D. C. Tsui, L. N. Pfeiffer, and K. W. West, Microwave Resonance of the Bubble Phases in 1/4 and 3/4 Filled High Landau levels, Phys. Rev. Lett. **89**, 136804 (2002).
[19] R. M. Lewis, Y. Chen, L. W. Engel, D. C. Tsui, P. D. Ye, L. N. Pfeiffer, and K. W. West, Evidence of a First-Order Phase Transition Between Wigner-Crystal and Bubble Phases of 2D Electrons in Higher Landau levels, Phys. Rev. Lett. **93**, 176808 (2004).
[20] B. Friess, Y. Peng, B. Rosenow, F. von Oppen, V. Umansky, K. von Klitzing, and J. H. Smet, Negative permittivity in bubble and stripe phases, Nat. Phys. **13**, 1124 (2017).
[21] B. Friess, V. Umansky, K. von Klitzing, and J. Smet, Current Flow in the Bubble and Stripe Phases, Phys. Rev. Lett. **120**, 137603 (2018).
[22] H. Deng, L. N. Pfeiffer, K. W. West, K. W. Baldwin, L. Engel, and M. Shayegan, Probing the Melting of a Two-Dimensional Quantum Wigner Crystal via its Screening Efficiency, Phys. Rev. Lett. **122**, 116601 (2019).
[23] M. K. Ma, K. A. Villegas Rosales, H. Deng, Y. Chung, L. N. Pfeiffer, K. W. West, K. Baldwin, R. Winkler, and M. Shayegan, Thermal and Quantum Melting Phase Diagrams for a Magnetic-Field-Induced Wigner Solid, Phys. Rev. Lett. **125**, 036601 (2020).
[24] J. P. Eisenstein, L. N. Pfeiffer, and K. W. West, Negative Compressibility of Interacting Two-Dimensional Electron and Quasiparticle Gases, Phys. Rev. Lett. **68**, 674 (1992).
[25] J. P. Eisenstein, L. N. Pfeiffer, and K. W. West, Compressibility of the two-dimensional electron gas: Measurements of the zero-field exchange energy and fractional quantum Hall gap, Phys. Rev. B **50**, 1760 (1994).
[26] Y. J. Chung, K. A. Villegas Rosales, K. W. Baldwin, K. W. West, M. Shayegan, and L. N. Pfeiffer, Working principles of doping-well structures for high-mobility two-dimensional electron systems, Phys. Rev. Materials **4**, 044003 (2020).
[27] At 15 K, we shine light with a red light emitting diode (LED) (next to the sample) for 30 min, and then proceed to mK temperatures. The illumination allows us to achieve optimum sample conditions (in terms of density and mobility).
[28] See Supplemental Material at http://link.aps.org/supplemental/10.1103/PhysRevB.104.L121110 for additional magnetoresistance and screening efficiency data, which includes Refs. [14,29–32].
[29] T. Sajoto, Y. P. Li, L. W. Engel, D. C. Tsui, and M. Shayegan, Hall Resistance of the Reentrant Insulating Phase around the 1/5 Fractional Quantum Hall Liquid, Phys. Rev. Lett. **70**, 2321 (1993).
[30] V. J. Goldman, J. K. Wang, B. Su, and M. Shayegan, Universality of the Hall Effect in a Magnetic-Field-Localized Two-Dimensional Electron System, Phys. Rev. Lett. **70**, 647 (1993).
[31] Y. J. Chung, K. A. Villegas Rosales, K. W. Baldwin, P. T. Madathil, K. W. West, M. Shayegan, and L. N. Pfeiffer, Ultra-high-quality two-dimensional electron systems, Nat. Mater. **20**, 632 (2021).
[32] S. Luryi, Quantum capacitance devices, Appl. Phys. Lett. **52**, 501 (1988).
[33] The reported I_P, which serves as a proxy for the screening efficiency, comes after calibrating the signal to remove the impact of parasitic capacitances. It is the out-of-phase (capacitive) component of the penetrating current.
[34] In the SM we report I_P vs ν at different fixed temperatures, also displaying the melting of bubble phases [28].
[35] Note that the parasitic capacitances and resistances (of, e.g., wires and contacts) have not been included.
[36] V. J. Goldman, M. Santos, M. Shayegan, and J. E. Cunningham, Evidence for Two-Dimensional Quantum Wigner Crystal, Phys. Rev. Lett. **65**, 2189 (1990).
[37] F. I. B. Williams, P. A. Wright, R. G. Clark, E. Y. Andrei, G. Deville, D. C. Glattli, O. Probst, B. Etienne, C. Dorin, C. T. Foxon, and J. J. Harris, Conduction Threshold and Pinning Frequency of Magnetically Induced Wigner Solid, Phys. Rev. Lett. **66**, 3285 (1991).
[38] M. A. Paalanen, R. L. Willett, R. R. Ruel, P. B. Littlewood, K. W. West, and L. N. Pfeiffer, Electrical conductivity and Wigner crystallization, Phys. Rev. B **45**, 13784(R) (1992).
[39] Y. P. Chen, G. Sambandamurthy, Z. Wang, R. Lewis, L. Engel, D. Tsui, P. Ye, L. Pfeiffer, and K. West, Melting of a 2D quantum electron solid in high magnetic field, Nat. Phys. **2**, 452 (2006).
[40] J. M. Kosterlitz and D. J. Thouless, Ordering, metastability and phase transitions in two-dimensional systems, J. Phys. C: Solid State Phys. **6**, 1181 (1973).
[41] B. I. Halperin and D. R. Nelson, Theory of Two-Dimensional Melting, Phys. Rev. Lett. **41**, 121 (1978).
[42] A. P. Young, Melting and the vector Coulomb gas in two dimensions, Phys. Rev. B **19**, 1855 (1979).
[43] D. Nelson and B. Halperin, Dislocation-mediated melting in two-dimensions, Phys. Rev. B **19**, 2457 (1979).
[44] R. Côté, C. B. Doiron, J. Bourassa, and H. A. Fertig, Dynamics of electrons in quantum Hall bubble phases, Phys. Rev. B **68**, 155327 (2003).
[45] M. O. Goerbig, P. Lederer, and C. M. Smith, Competition between quantum-liquid and electron-solid phases in intermediate Landau levels, Phys. Rev. B **69**, 115327 (2004).
[46] D. Ro, N. Deng, J. D. Watson, M. J. Manfra, L. N. Pfeiffer, K. W. West, and G. A. Csathy, Electron bubbles and the structure of the orbital wave function, Phys. Rev. B **99**, 201111(R) (2019).
[47] D. Ro, S. A. Myers, N. Deng, J. D. Watson, M. J. Manfra, L. N. Pfeiffer, K. W. West, and G. A. Csáthy, Stability of multielectron bubbles in high Landau levels, Phys. Rev. B **102**, 115303 (2020).